Lattice Structures for Optimal Design and Robust Implementation of Two-Channel Perfect-Reconstruction QMF Banks

P. P. VAIDYANATHAN, MEMBER, IEEE, AND PHUONG-QUAN HOANG, STUDENT MEMBER, IEEE

Abstract—**A lattice structure and an algorithm are presented for the design of two-channel QMF banks, satisfying a sufficient condition for perfect reconstruction. The structure inherently has the perfect-reconstruction property, while the algorithm ensures a good stopband attenuation for each of the analysis filters. Implementations of such lattice structures are robust in the sense that the perfect-reconstruction property is preserved in spite of coefficient quantization. The lattice structure has a hierarchical property, in the sense that a higher order perfect-reconstruction QMF bank can be obtained from a lower order perfect-reconstruction QMF bank, simply by adding more lattice sections. Several numerical examples are provided in the form of design tables.**

I. Introduction

THE problem of quadrature mirror filtering (QMF) has received substantial attention recently [1]–[14]. These filters find application when a signal is to be split into two or more frequency bands, with each band subsequently processed in an independent manner. Fig. 1 shows a two-band QMF bank where $H_0(z)$ and $H_1(z)$ are the "analysis filters" (low-pass and high-pass, respectively). The subband signals $x_0(n)$ and $x_1(n)$ are undersampled (or "decimated") by a factor of two, then transmitted after possible encoding [2]. At the receiver end, the signals are upsampled, filtered, and recombined to produce the reconstructed signal $\hat{x}(n)$. In order to avoid a spectral gap, the responses $H_0(e^{j\omega})$ and $H_1(e^{j\omega})$ inevitably overlap, and this causes aliasing when the signals are decimated. The "synthesis bank" filters $F_0(z)$ and $F_1(z)$ are usually designed such that this aliasing effect is cancelled by the "imaging" effect of interpolators [2].

The most general relation between $\hat{X}(z)$ and $X(z)$ in Fig. 1 is given by [2]:

$$\hat{X}(z) = \tfrac{1}{2}\left[H_0(z)\,F_0(z) + H_1(z)\,F_1(z)\right]X(z) + \tfrac{1}{2}\left[H_0(-z)\,F_0(z) + H_1(-z)\cdot F_1(z)\right]X(-z). \quad (1)$$

Manuscript received March 28, 1987; revised July 15, 1987. This work was supported in part by the National Science Foundation under Grant DCI 8552579, by the matching funds provided by Pacific Bell and General Electric Co., by Caltech's Programs in Advanced Technology Grant sponsored by Aerojet General, General Motors, GTE and TRW, and by the National Science Foundation under Grant MIP 8604456.

The authors are with the Department of Electrical Engineering, California Institute of Technology, Pasadena, CA 91125.

IEEE Log Number 8717672.

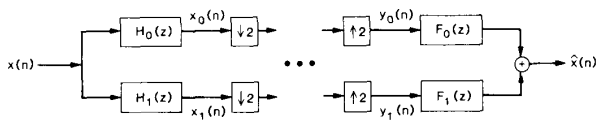

Fig. 1. A two-channel QMF bank.

It is well known [1]–[3] that the choice of synthesis filters $F_k(z)$ according to

$$F_0(z) = -H_1(-z), \qquad F_1(z) = H_0(-z) \quad (2)$$

cancels the aliasing term [second term in (1)], leading to the result

$$T(z) = \frac{\hat{X}(z)}{X(z)} = \frac{1}{2}\left[-H_0(z)\,H_1(-z) + H_1(z)\,H_0(-z)\right]. \quad (3)$$

Once aliasing is thus cancelled, the QMF bank is a time-invariant system characterized by the transfer function $T(z)$. Thus, in general, the reconstructed signal $\hat{X}(z)$ suffers from amplitude distortion (due to nonconstant $|T(e^{j\omega})|$) and phase distortion (due to nonlinear arg $[T(e^{j\omega})]$). It has been known for some time how phase or amplitude distortion can be completely eliminated [2], [13]–[15], [5].

It has recently been established [4] that, in the QMF bank of Fig. 1, amplitude and phase distortion can *both* be simultaneously eliminated, thereby resulting in a perfect-reconstruction QMF bank, while at the same time obtaining any arbitrary prespecified stopband attenuation for the analysis filter. Such a system satisfies

$$\hat{x}(n) = c \cdot x(n - n_0) \quad (4)$$

where c is a constant and n_0 is a positive integer.

In this paper, we consider such two-channel perfect-reconstruction systems. Two aspects of such systems will be considered: design of the transfer functions $H_k(z)$ and implementation based on a new family of lattice structures. Quantization and roundoff noise effects in these structures are analyzed as well.

Before outlining the purpose of this paper, let us briefly recapitulate the design procedure described in [4] for accomplishing perfect reconstruction. First, a linear-phase FIR half-band low-pass filter $G(z)$ is designed. Such a

filter has frequency response

$$G(e^{j\omega}) = \exp\left[-j\omega(N-1)\right] G_0(e^{j\omega}) \qquad (5)$$

where $2(N-1)$ is the order of the filter, and $G_0(e^{j\omega})$ is the real-valued zero-phase response (or "amplitude response"). Without loss of generality [11, p. 485], we assume that $N-1$ is odd. Fig. 2 shows a plot of $G_0(e^{j\omega})$ (solid curve). Notice the symmetry with respect to the frequency $\pi/2$, which can be expressed as

$$G(z) - G(-z) = c \cdot z^{-(N-1)}. \qquad (6)$$

In this paper, the term "half-band filter" is used to describe linear-phase FIR filters satisfying (6) for some constant c. Condition (6) automatically implies $\omega_p + \omega_s = \pi$ and implies that the passband error curve is an image of the stopband error curve with respect to $\pi/2$.

Given the half-band filter $G(z)$ with response $G_0(e^{j\omega})$ as in Fig. 2 (solid curve), it is possible to design a half-band filter $G_+(z)$ with positive amplitude response $G_{+,0}(e^{j\omega})$ (dashed curve) simply by defining $G_+(z) = G(z) + \delta z^{-(N-1)}$. The function $G_+(z)$ can therefore be factorized as $G_+(z) = z^{-(N-1)}H_0(z^{-1})\,H_0(z)$, where $H_0(z)$ is an FIR low-pass function of order $N-1$ having real-valued impulse response coefficients. With $H_0(z)$ designed in this manner, the choice

$$\begin{aligned} H_1(z) &= z^{-(N-1)}H_0(-z^{-1}), \\ F_0(z) &= z^{-(N-1)}H_0(z^{-1}), \\ F_1(z) &= z^{-(N-1)}H_1(z^{-1}) \end{aligned} \qquad (7)$$

results in perfect reconstruction [4], since aliasing is cancelled and (3) reduces to a delay.

$H_0(z)$ and $H_1(z)$, as designed, form a power-complementary pair, i.e., they satisfy

$$H_0(z)\,H_0(z^{-1}) + H_1(z)\,H_1(z^{-1}) = d \qquad (8)$$

for some constant d, and therefore cannot *both* have linear phase [24]. In two-channel QMF banks with linear-phase analysis filters, it is possible to obtain perfect reconstruction as indicated in [23]. However, the attenuation characteristics of such linear-phase analysis filters seem to be poor (also see Section VI for further remarks).

In an actual implementation of Fig. 1, the coefficients of $H_k(z)$ and $F_k(z)$ should be quantized (for example, in a *direct form* implementation, the *impulse response* coefficients are quantized). In spite of this, relation (7) continues to be true because the multiplier coefficients in $H_1(z)$, $F_0(z)$, and $F_1(z)$ are the same as those in $H_0(z)$ (except for the reordering and sign reversal operations). However, once the coefficients are quantized, $H_0(z)$ does not remain a spectral factor of a half-band filter, and consequently (3) does not reduce to a delay. Thus, even though aliasing continues to be absent, the perfect-reconstruction property is actually lost.

The natural question that arises is this: does there exist a structure for implementing the analysis banks such that $H_0(z)$ remains a spectral factor of a half-band filter (with positive amplitude response) in spite of coefficient quantization? The answer is in the affirmative and such a structure is introduced in Section II of this paper. Equation (8) holds for this structure regardless of the extent of coefficient quantization. This result is new, compared to those in [11], although the new structure is derivable from those treated in [11].

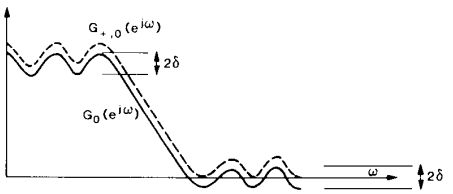

Fig. 2. The amplitude responses of the linear-phase half-band filters $G(z)$ and $G_+(z)$.

With α_k denoting the multiplier coefficients in the new structure, (7) and (8) are satisfied unconditionally for all values of α_k. Accordingly, perfect reconstruction [i.e., (4)] is "structurally induced." The structure therefore forms an ideal candidate, not only for implementation purposes, but also for an optimization strategy in designing $H_0(z)$. This procedure is desirable especially for large values of $N-1$ when the spectral factorization becomes increasingly inaccurate and time consuming, particularly in view of the fact that there are many zeros of $G_+(z)$ on the unit circle.

The organization of this paper is as follows. In Section II, the new lattice structures are presented along with a proof of the structurally induced, perfect-reconstruction property, and the relation to the half-band filters is reestablished. Section III presents an optimization algorithm for directly designing $H_0(z)$ based on lattice parameters. According to our experience, the results always yield filters with the maximum possible number of stopband zeros on the unit circle (see Appendix A for an expression for this number), under the constraints of (7) and (8). Moreover, the peak error in the stopband is monotone decreasing (rather than equiripple) which is often considered to be an advantage [2], [14]. Section IV presents design examples, along with computer simulation of quantization effects. Even though the perfect-reconstruction property remains intact in spite of quantization, the stopband attenuation of $H_k(z)$ decreases with increased quantization, but the effects are quite acceptable, as shown by simulation examples. Section V includes roundoff noise analysis for the QMF structure. The effect of decimators and interpolators makes the analysis interesting because of the apparent "nonstationarity" of the roundoff noise sequence. The "losslessness" property of the lattice structure, however, renders the computation of noise-gain relatively simple. In Appendix B, we show that the lattice has about the same relative error in the stopband as in the passband; since the lattice has low passband sensitivity [6], this provides an upper bound on the quantization effect in the stopband. Appendix C includes a short software program which computes the impulse response coefficients from a given set of lattice coefficients α_k. In Tables I–VII, we have included numerical design exam-

TABLE I
DESIGN DETAILS FOR THE LATTICE FILTERS

Filter Number N length	ω_s specified (π radians)	ω_s measured (π radians)	Transition Bandwidth $\omega_s - \frac{(\pi/2)}{2\pi}$	Stopband Attenuation (First Peak) (dB)	Stopband Attenuation (Last Peak) (dB)
8A	0.78	0.795	0.1474	41	43
12A	0.78	0.787	0.1434	58	61
16A	0.78	0.781	0.1407	75	79
12B	0.70	0.715	0.1075	41	44
16B	0.70	0.709	0.1045	52	56
24B	0.70	0.702	0.1010	74	81
16C	0.62	0.635	0.0673	33	39
24C	0.62	0.626	0.0630	45	53
32C	0.62	0.623	0.0617	57	67
48C	0.62	0.623	0.0613	85	89
16F	0.60	0.619	0.0597	29	35
24F	0.60	0.608	0.0540	38	47
32F	0.60	0.605	0.0527	49	59
48F	0.60	0.602	0.0510	70	82
24D	0.58	0.590	0.0450	32	41
32D	0.58	0.587	0.0433	40	51
48D	0.58	0.582	0.0410	56	69
64D	0.58	0.580	0.0400	74	88
70D	0.58	0.580	0.0400	81	88
32E	0.54	0.553	0.0267	25	37
48E	0.54	0.546	0.0230	32	49
64E	0.54	0.543	0.0217	40	56

TABLE II
VALUES OF α_m FOR OPTIMAL FILTERS

	Filter #8A	Filter #12A	Filter #12B
α_1	−0.2638026e−01	−0.3676246e+01	−0.3096168e+01
α_2	0.7154463e+00	0.1100022e+01	0.9370946e+00
α_3	−0.2598479e+00	−0.5170637e+00	−0.4569771e+00
α_4	0.6388361e−01	0.2362183e+00	0.2276283e+00
α_5		−0.8441314e−01	−0.9712722e−01
α_6		0.1716341e−01	0.2795064e−01

TABLE III
VALUES OF α_m FOR OPTIMAL FILTERS

	Filter #16A	Filter #16B	Filter #16C	Filter #16F
α_1	−0.4699145e+01	−0.3886354e+01	−0.2966504e+01	−0.2739714e+01
α_2	0.1465103e+01	0.1218756e+01	0.9334946e+00	0.8611533e+00
α_3	−0.7597957e+00	−0.6429331e+00	−0.5028173e+00	−0.4660051e+00
α_4	0.4216733e+00	0.3707214e+00	0.3051719e+00	0.2868931e+00
α_5	−0.2181804e+00	−0.2068881e+00	−0.1879673e+00	−0.1817166e+00
α_6	0.9405991e−01	0.1023296e+00	0.1104991e+00	0.1120899e+00
α_7	−0.2924380e−01	−0.4016767e−01	−0.5811574e−01	0.6389849e−01
α_8	0.4905888e−02	0.9948452e−02	0.2437997e−01	0.3098943e−01

TABLE IV
VALUES OF α_m FOR OPTIMAL FILTERS

	Filter #24B	Filter #24C	Filter #24F	Filter #24D
α_1	0.5462615e+01	0.3965091e+01	−0.3587773e+01	−0.3219439e+01
α_2	0.1765271e+01	0.1282368e+01	0.1158946e+01	0.1037174e+01
α_3	−0.9933745e+00	−0.7260119e+00	0.6565104e+00	0.5871553e+00
α_4	0.6405501e+00	0.4756307e+00	0.4319230e+00	0.3877585e+00
α_5	−0.4290425e+00	−0.3284689e+00	−0.3010528e+00	0.2728663e+00
α_6	0.2844221e+00	0.2293814e+00	0.2135914e+00	0.1968799e+00
α_7	−0.1798644e+00	−0.1576285e+00	−0.1504406e+00	0.1423481e+00
α_8	0.1045704e+00	0.1040772e+00	0.1030309e+00	0.1013140e+00
α_9	−0.5351832e−01	−0.6431627e−01	−0.6712935e−01	0.6975467e−01
α_{10}	0.2273594e−01	0.3591622e−01	0.4045162e−01	0.4548290e−01
α_{11}	−0.7266256e−02	−0.1709523e−01	−0.2154214e−01	−0.2720419e−01
α_{12}	0.1373516e−02	0.6056575e−02	0.9188643e−02	0.1403098e−01

TABLE V
VALUES OF α_m FOR OPTIMAL FILTERS

	Filter #32C	Filter #32F	Filter #32D	Filter #32E
α_1	0.4947162e+01	0.4419554e+01	−0.3897719e+01	0.2937657e−01
α_2	0.1618750e+01	0.1444868e+01	0.1271721e+01	0.9474481e−00
α_3	−0.9366921e+00	−0.8358118e+00	−0.7345884e−00	0.5416029e−00
α_4	0.6339676e−00	0.5664486e−00	0.4981979e−00	0.3658746e−00
α_5	0.4583882e−00	0.4110873e−00	−0.3628759e−00	0.2676719e−00
α_6	0.3411142e−00	0.3079806e−00	0.2738343e−00	0.2048268e−00
α_7	0.2558051e−00	0.2334207e+00	−0.2099638e−00	0.1610002e−00
α_8	0.1904199e−00	0.1764921e+00	0.1614840e+00	0.1285583e−00
α_9	0.1388874e−00	−0.1316083e+00	0.1233244e+00	0.1034792e−00
α_{10}	0.9798419e−01	0.9572774e−01	0.9266412e−01	0.8345957e−01
α_{11}	0.6591964e−01	0.6712079e−01	0.6785856e−01	0.6709826e−01
α_{12}	0.4157153e−01	0.4473385e−01	0.4790362e−01	0.5350337e−01
α_{13}	0.2402169e−01	0.2781714e−01	0.3211141e−01	0.4208714e−01
α_{14}	0.1228736e−01	0.1569589e−01	0.2007797e−01	0.3245102e−01
α_{15}	0.5221147e−02	0.7645295e−02	0.1127087e−01	0.2431732e−01
α_{16}	0.1576151e−02	0.2854061e−02	0.5264834e−02	0.1748662e−01

TABLE VI
VALUES OF α_m FOR OPTIMAL FILTERS

	Filter #48C	Filter #48F	Filter #48D	Filter #48E
α_1	−0.6315784e+01	−0.6057506e+01	−0.5228952e+01	−0.3836487e−01
α_2	0.2088393e+01	0.2000152e+01	0.1724735e+01	0.1247866e−01
α_3	−0.1232629e+01	−0.1178251e+01	−0.1014721e−01	−0.7220668e+00
α_4	0.8584247e+00	0.8193606e+00	0.7051436e−00	0.4951553e+00
α_5	−0.6447275e+00	−0.6152533e+00	−0.5296424e+00	−0.3688423e+00
α_6	0.5040390e+00	0.4817286e+00	0.4153386e+00	0.2885146e+00
α_7	−0.4027649e+00	−0.3863457e+00	−0.3341087e+00	−0.2327588e+00
α_8	0.3252960e+00	0.3139650e+00	0.2728079e+00	0.1913137e+00
α_9	−0.2634520e+00	−0.2566057e+00	−0.2244915e+00	−0.1598938e+00
α_{10}	0.2125983e+00	0.2097031e+00	0.1851713e+00	0.1348106e+00
α_{11}	0.1699807e+00	−0.1705025e+00	−0.1524203e+00	−0.1140321e+00
α_{12}	0.1339247e+00	0.1372864e+00	0.1247027e+00	0.9681786e−01
α_{13}	0.1034047e+00	−0.1089672e+00	−0.1010221e+00	−0.8223478e−01
α_{14}	0.7778612e−01	0.8485096e−01	0.8072150e−01	0.6963367e−01
α_{15}	−0.5664952e−01	−0.6448664e−01	−0.6336105e−01	−0.5867790e−01
α_{16}	0.3966167e−01	0.4756036e−01	0.4863688e−01	0.4913793e−01
α_{17}	−0.2648138e−01	0.3381633e−01	−0.3632357e−01	0.4081778e−01
α_{18}	0.1670176e−01	0.2299884e−01	0.2623183e−01	0.3353566e−01
α_{19}	−0.9831959e−02	0.1481523e−01	−0.1817794e−01	−0.2713113e−01
α_{20}	0.5316054e−02	0.8920900e−02	0.1196394e−01	0.2149517e−01
α_{21}	−0.2578539e−02	−0.4925761e−02	−0.7368346e−02	0.1658255e−01
α_{22}	0.1079437e−02	0.2417364e−02	0.4146564e−02	0.1238607e−01
α_{23}	−0.3618121e−03	−0.9931265e−03	−0.2039489e−02	0.8895189e−02
α_{24}	0.7954759e−04	0.2925763e−03	0.7873639e−03	0.6072120e−02

ples. Basically, for a given stopband edge and stopband attenuation, the set of lattice coefficients α_k that gives rise to the "best filter" $H_0(z)$ in an L_2 sense is tabulated. This is therefore a quick design aid, and saves the designer from recomputing standard coefficients by elaborate optimization algorithms.

Notations: In this paper, superscript t stands for matrix transposition. Bold-faced italic letters indicate vectors and matrices. The tilde accent stands for transposition followed by reciprocation of functional argument; for example, $\tilde{\boldsymbol{H}}(z) = \boldsymbol{H}^t(z^{-1})$. On the unit circle, this is equivalent to transposed conjugation.

II. THE QMF LATTICE STRUCTURE

In a recent paper [6], a new class of nonrecursive cascaded lattice structures was introduced for the implemen-

TABLE VII
VALUES OF α_m FOR OPTIMAL FILTERS

	Filter #64D	Filter #64E	Filter #70D
α_1	0.6541668e-01	0.4327252e-01	-0.6404257e+01
α_2	0.2167132e-01	0.1425816e-01	0.2126039e-01
α_3	0.1284988e-01	0.8392532e-00	-0.1265223e+01
α_4	0.9024673e-00	0.5855141e-00	0.8926746e+00
α_5	0.6869024e-00	0.4435185e+00	0.6829382e-00
α_6	0.5474343e-00	0.3525763e-00	0.5472484e-00
α_7	0.4490405e+00	0.2891957e-00	0.4514609e+00
α_8	0.3753422e-00	0.2423609e+00	0.3796413e+00
α_9	-0.3176566e-00	0.2062240e+00	0.3233572e-00
α_{10}	0.2709592e-00	0.1773966e-00	0.2777332e-00
α_{11}	0.2321494e+00	0.1537840e-00	0.2397611e+00
α_{12}	0.1992207e-00	0.1340248e+00	0.2074910e-00
α_{13}	-0.1708276e-00	-0.1171987e-00	0.1796115e-00
α_{14}	0.1460453e-00	0.1026636e-00	0.1552163e+00
α_{15}	0.1242279e-00	-0.8996029e-01	-0.1336672e+00
α_{16}	0.1049204e-00	0.7875330e-01	0.1145095e-00
α_{17}	-0.8780164e-01	0.6879375e-01	0.9741762e-01
α_{18}	0.7264466e-01	0.5989449e-01	0.8215835e-01
α_{19}	-0.5928753e-01	-0.5191327e-01	0.6856392e-01
α_{20}	0.4761084e-01	0.4474097e-01	0.5651222e-01
α_{21}	0.3751935e-01	-0.3829306e-01	-0.4591068e-01
α_{22}	0.2892705e-01	0.3250329e-01	0.3668317e-01
α_{23}	0.2174538e-01	-0.2731889e-01	-0.2875914e-01
α_{24}	0.1587490e-01	0.2269681e-01	0.2206526e-01
α_{25}	0.1120080e-01	-0.1860079e-01	-0.1651930e-01
α_{26}	0.7592156e-02	0.1499897e-01	0.1202692e-01
α_{27}	0.4901821e-02	-0.1186202e-01	-0.8481189e-02
α_{28}	0.2987045e-02	0.9161671e-02	0.5764517e-02
α_{29}	0.1686799e-02	0.6869633e-02	0.3752771e-02
α_{30}	0.8595028e-03	0.4956829e-02	0.2320577e-02
α_{31}	0.3719419e-03	0.3392964e-02	0.1347041e-02
α_{32}	0.1221688e-03	0.2146366e-02	0.7210611e-03
α_{33}			0.3549222e-03
α_{34}			0.1398132e-03
α_{35}			0.4105982e-04

tation of FIR digital filters. These structures, shown in Fig. 3, can be used for the synthesis of *any* scalar FIR transfer function $H(z)$ with no restriction on the location of the zeros. In Fig. 3, $\hat{k}_m$ are such that $\hat{k}_m^2 + k_m^2 = 1$; thus, the lattice coefficients k_m and $\hat{k}_m$ have magnitudes bounded above by unity. Fig. 4 shows a "denormalized" implementation, obtained by defining $\gamma_m = \hat{k}_m/k_m$ and introducing the scale factors $\beta = k_1 k_2 \cdots k_{N-1}$ (or, equivalently, $\beta^2 = \Pi_{i=1}^{N-1}(1 + \gamma_i^2)^{-1}$). Here, the magnitudes of γ_m are no longer bounded above by unity. For convenience of future notation, in Fig. 4, after each lattice section, we denote the pair of "unscaled" transfer functions by $P_m(z)$, $Q_m(z)$ (notice that the subscript m also indicates the order of the transfer functions). The transfer functions $H_0(z) \triangleq \hat{P}_{N-1}(z)$ and $H_1(z) \triangleq \hat{Q}_{N-1}(z)$ are given by $\hat{P}_{N-1}(z) = \beta P_{N-1}(z)$, $\hat{Q}_{N-1}(z) = \beta Q_{N-1}(z)$. It can be shown [6] that the lattice structures of Figs. 3 and 4 satisfy the "power complementary property" [17]

$$\left|H_0(e^{j\omega})\right|^2 + \left|H_1(e^{j\omega})\right|^2 = d \qquad (9)$$

where d is some constant depending upon the multipliers in the structure. For Fig. 3, $d = 1$ if k_m and $\hat{k}_m$ satisfy $k_m^2 + \hat{k}_m^2 = 1$ exactly (which is not possible when these coefficients have finite wordlength). The significant fact, however, is that d is constant, and that (9) implies (8) by

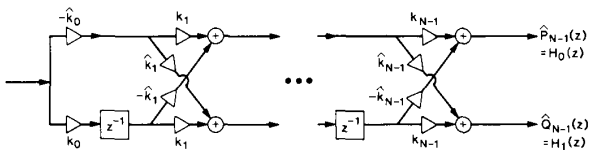

Fig. 3. The cascaded lattice structure.

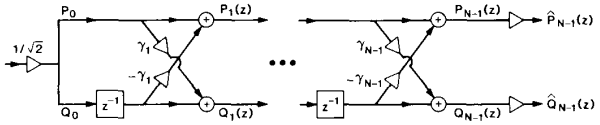

Fig. 4. A "denormalized" implementation of the cascaded lattice structure.

analytic continuation (assuming real impulse responses). This observation suggests that the lattice structure will generate appropriate analysis filter transfer functions $H_0(z)$ and $H_1(z)$ for the perfect-reconstruction QMF bank, as long as they satisfy the further condition

$$H_1(z) = z^{-(N-1)}H_0(-z^{-1}), \qquad (10)$$

as required by (7). Conditions (9) and (10) [or equivalently, (8) and (10)] are precisely the conditions satisfied by the analysis filters in [4]. In this paper, this pair of conditions will be jointly referred to as the "power-complementary image condition" (PCI condition), and if the pair $\{H_0(z), H_1(z)\}$ satisfies the PCI condition, we will call it the "power-complementary image pair" (PCI pair). Note that the PCI condition is sufficient for perfect reconstruction, but not necessary (Section VI).

In a design example of this type of lattice structure which was reported in [6], the following observation was made (without proof): if the lattice transfer functions satisfy (10) then the coefficients k_m satisfy

$$k_0^2 = \hat{k}_0^2 = \tfrac{1}{2}, \qquad k_{2m}^2 = 1 \text{ for } m > 0. \qquad (11)$$

In terms of γ_m, the relation (11) is equivalent to

$$\gamma_0^2 = 1, \qquad \gamma_{2m} = 0 \text{ for } m > 0. \qquad (12)$$

In other words, the lattice structure can be redrawn as in Fig. 5. In this section, we will formally show that the lattice structure satisfies (12) *if and only if* the transfer functions $H_0(z)$, $H_1(z)$ satisfy the PCI condition. The importance of this observation is that the structure of Fig. 5 generates a PCI pair regardless of the values of γ_1, γ_3, $\cdots$, etc. Accordingly, quantization of γ_k in Fig. 5 does not affect the PCI property.

Let us first prove by induction that if relation (12) holds, that is, if the lattice structure of Fig. 4 reduces to the form in Fig. 5, then the lattice transfer functions satisfy the PCI condition. For this, we show that, in Fig. 5, if $\{P_{m-1}(z), Q_{m-1}(z)\}$ is a PCI pair then so is $\{P_{m+1}(z), Q_{m+1}(z)\}$. The basis for the inductive argument can be established by noting that $\{P_0(z), Q_0(z)\}$ and $\{P_1(z), Q_1(z)\}$ which

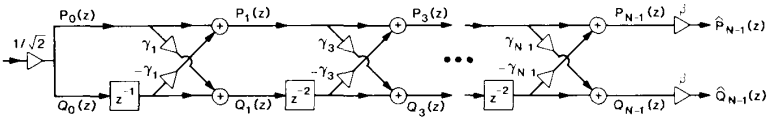

Fig. 5. The QMF lattice, pertaining to the proof in Section II.

are given by

$$P_0(z) = Q_0(z) = \frac{1}{\sqrt{2}},$$

$$\begin{pmatrix} P_1(z) \\ Q_1(z) \end{pmatrix} = \begin{pmatrix} 1 & -\gamma_1 \\ \gamma_1 & 1 \end{pmatrix} \begin{pmatrix} P_0(z) \\ z^{-1}Q_0(z) \end{pmatrix}$$

are PCI pairs. Now suppose that the pair $\{P_{m-1}, Q_{m-1}\}$, where $m-1$ is odd, satisfies the PCI condition. The lattice structure relates $\{P_{m+1}(z), Q_{m+1}(z)\}$ to $\{P_{m-1}(z), Q_{m-1}(z)\}$ as follows:

$$\begin{pmatrix} P_{m+1}(z) \\ Q_{m+1}(z) \end{pmatrix} = \begin{pmatrix} 1 & -\gamma_{m+1} \\ \gamma_{m+1} & 1 \end{pmatrix} \cdot \begin{pmatrix} P_{m-1}(z) \\ z^{-2}Q_{m-1}(z) \end{pmatrix}. \quad (13)$$

From (13)

$$\tilde{P}_{m+1}(z)\,P_{m+1}(z) + \tilde{Q}_{m+1}(z)Q_{m+1}(z) = (1+\gamma_{m+1}^2)\left\{\tilde{P}_{m-1}(z)\,P_{m-1}(z) + \tilde{Q}_{m-1}(z)Q_{m-1}(z)\right\} = \text{constant}.$$

Thus, $\{P_{m+1}(z), Q_{m+1}(z)\}$ satisfies relation (9). From (13), $Q_{m+1}(z) = \gamma_{m+1}P_{m-1}(z) + z^{-2}Q_{m-1}(z) = -\gamma_{m+1}z^{-(m-1)}Q_{m-1}(-z^{-1}) + z^{-2}z^{-(m-1)}P_{m-1}(-z^{-1}) = z^{-(m+1)}P_{m+1}(-z^{-1})$. Therefore, $\{P_{m+1}(z), Q_{m+1}(z)\}$ satisfies a relation of the form (10). So $\{P_{m+1}(z), Q_{m+1}(z)\}$ is a PCI pair. This shows that, in the lattice of Fig. 5, every pair $\{P_{2m-1}(z), Q_{2m-1}(z)\}$, $m = 1, 2, \cdots, N/2$, satisfies the PCI condition.

We now prove the converse, that is, if the lattice transfer functions in Fig. 4 satisfy the PCI condition, then relation (12) holds, so that the lattice reduces to the form in Fig. 5. First observe that, without loss of generality, the order of the transfer functions $N-1$ can be assumed to be odd [11, p. 485]. Assume that $\{P_{m+1}(z), Q_{m+1}(z)\}$, where $m+1$ is odd, is a PCI pair, i.e.,

$$\tilde{P}_{m+1}(z)\,P_{m+1}(z) + \tilde{Q}_{m+1}(z)Q_{m+1}(z) = \text{constant} \quad (14)$$

$$Q_{m+1}(z) = z^{-(m+1)}P_{m+1}(-z^{-1}), \quad (15)$$

where $P_{m+1}(z) = \Sigma_{i=0}^{m+1} z^{-i}p_{m+1,i}$ and $Q_{m+1}(z) = \Sigma_{i=0}^{m+1} z^{-i}q_{m+1,i}$. Assume that

$$p_{m+1,0}p_{m+1,m+1} \neq 0, \quad (16)$$

so that $P_{m+1}(z)$ has order $m+1$, and has a nonzero constant term. Now, (14) implies $p_{m+1,0}p_{m+1,m+1} + q_{m+1,0}q_{m+1,m+1} = 0$, hence, (16) also implies that $q_{m+1,0}q_{m+1,m+1} \neq 0$, i.e., $Q_{m+1}(z)$ also has order $m+1$ and a nonzero constant term. We first show that $\{P_m(z), Q_m(z)\}$ is also a PCI pair. Let $P_m(z) = \Sigma_{i=0}^{m} z^{-i}p_{m,i}$ and $Q_m(z) = \Sigma_{i=0}^{m} z^{-i}q_{m,i}$. The lattice structure relates $P_m(z)$ and $Q_m(z)$ to $P_{m+1}(z)$ and $Q_{m+1}(z)$ as follows:

$$\begin{pmatrix} P_m(z) \\ z^{-1}Q_m(z) \end{pmatrix} = \frac{1}{1+\gamma_{m+1}^2} \cdot \begin{pmatrix} 1 & \gamma_{m+1} \\ -\gamma_{m+1} & 1 \end{pmatrix} \begin{pmatrix} P_{m+1}(z) \\ Q_{m+1}(z) \end{pmatrix}. \quad (17)$$

Since the 2×2 matrix in (17) is orthogonal, we can readily verify, based on (14), that $\{P_m(z), Q_m(z)\}$ is a power complementary pair, i.e.,

$$\tilde{P}_m(z)\,P_m(z) + \tilde{Q}_m(z)Q_m(z) = \text{constant}. \quad (18)$$

Let us prove that it also satisfies a relation similar to (15). Equation (17) gives

$$(1+\gamma_{m+1}^2)\,P_m(-z^{-1}) = P_{m+1}(-z^{-1}) + \gamma_{m+1}Q_{m+1}(-z^{-1}).$$

In view of (15) and the assumption that $m+1$ is odd, $Q_{m+1}(-z^{-1}) = -z^{m+1}P_{m+1}(z)$. So we have $(1+\gamma_{m+1}^2)\,P_m(-z^{-1}) = z^{m+1}\{Q_{m+1}(z) - \gamma_{m+1}P_{m+1}(z)\} = z^{m+1}\{(1+\gamma_{m+1}^2)\,z^{-1}\,Q_m(z)\}$. Therefore, $\{P_m(z), Q_m(z)\}$ is a PCI pair, i.e., it satisfies (18) and

$$Q_m(z) = z^{-m}P_m(-z^{-1}). \quad (19)$$

We now prove that $p_{m,m} = q_{m,0} = 0$, i.e., $P_m(z)$ is actually of order $m-1$, and $Q_m(z)$ can be expressed as $z^{-1}Q_{m-1}(z)$. In other words, the structure of Fig. 4 reduces to that of Fig. 5. Equation (18) implies, in particular, that

$$p_{m,0}p_{m,m} + q_{m,0}q_{m,m} = 0. \quad (20)$$

Equation (19) implies that

$$q_{m,0} = (-1)^{-m}p_{m,m}, \qquad q_{m,m} = p_{m,0}. \quad (21)$$

From (20) and (21) we obtain $p_{m,0}p_{m,m} = 0$ (since $m+1$ is odd). Equation (17) describes the process of reducing the order of $P_{m+1}(z)$ and $Q_{m+1}(z)$ by 1. For this order reduction to take place, it is clear that we must have

$$p_{m+1,m+1} + \gamma_{m+1}q_{m+1,m+1} = 0, \quad \text{i.e.,}$$

$$\gamma_{m+1} = -p_{m+1,m+1}/q_{m+1,m+1}, \quad (22)$$

where $q_{m+1,m+1}$, by assumption, is nonzero. From (17) and (22), we have $p_{m,0} = (p_{m+1,0} - p_{m+1,m+1}q_{m+1,0}/q_{m+1,m+1})/(1+\gamma_{m+1}^2)$. Using (21) we see that if $p_{m,0} = 0$, then $p_{m+1,0}^2 = -p_{m+1,m+1}^2$, which violates (16). So

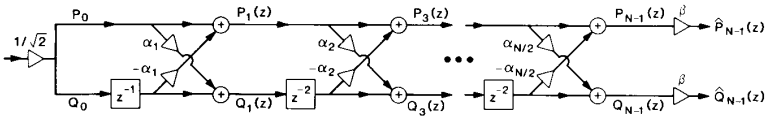

Fig. 6. The QMF lattice, with $\alpha_m = \gamma_{2m-1}$.

we must have $p_{m,0} \neq 0$, hence, $p_{m,m} = q_{m,0} = 0$. Thus, if we define

$$P_{m-1}(z) = P_m(z), \qquad Q_{m-1}(z) = zQ_m(z) \quad (23)$$

then all the conditions satisfied by the pair $\{P_{m+1}(z), Q_{m+1}(z)\}$ are also satisfied by $\{P_{m-1}(z), Q_{m-1}(z)\}$. If $p_{m-1,m-1}$ turns out to be zero, then two more stages will be skipped. Otherwise, the upward recursion continues until we obtain

$$\begin{aligned} P_1(z) &= p_{1,0} + z^{-1}p_{1,1} \\ Q_1(z) &= -p_{1,1} + z^{-1}p_{1,0} \\ P_0(z) &= Q_0(z) = \frac{1}{\sqrt{2}}. \end{aligned} \quad (24)$$

This concludes the proof that if $\{P_{N-1}(z), Q_{N-1}(z)\}$ satisfies the PCI condition, then the lattice in Fig. 5 realizes it.

For the rest of this paper, we shall be concerned only with the class of lattice structures in Fig. 5 which we call "the QMF lattice." For ease of future notation, the QMF lattice is redrawn as in Fig. 6, where $\alpha_m = \gamma_{2m-1}$.

Relation Between the QMF Lattice and Half-Band Filters with Positive Amplitude Responses: We have proved that the transfer functions $\hat{P}_{N-1}(z)$ and $\hat{Q}_{N-1}(z)$ of the QMF lattice, with $N-1$ odd, satisfy the PCI condition, viz., (18) and (19), for $m = N-1$. Now let

$$G_+(z) = z^{-(N-1)}\hat{P}_{N-1}(z^{-1})\,\hat{P}_{N-1}(z). \quad (25)$$

Relation (25) shows that $G_+(z)$ is a linear-phase filter having nonnegative zero-phase (or "amplitude") response. From (25), $G_+(-z) = -z^{-(N-1)}\hat{P}_{N-1}(-z^{-1})\,\hat{P}_{N-1}(-z) = -z^{-(N-1)}\hat{Q}_{N-1}(z)\,\hat{Q}_{N-1}(z^{-1})$. Therefore,

$$G_+(z) - G_+(-z) = z^{-(N-1)} \cdot \text{constant}, \quad (26)$$

which means that $G_+(z)$ is a half-band filter. In other words, $\hat{P}_{N-1}(z)$ and $\hat{Q}_{N-1}(z)$ are spectral factors of $G_+(z)$ and $G_+(-z)$, respectively, which are half-band filters of order $2(N-1)$, with positive amplitude responses.

III. The Complete QMF Bank

The analysis bank is now as in Fig. 6, which can be drawn in the form of Fig. 7, where $\boldsymbol{E}(z)$ is a 2×2 transfer matrix. Since each lattice section in Fig. 6 is orthogonal, the transfer matrix $\boldsymbol{E}(z)$ is unitary on the unit circle. More generally, $\boldsymbol{E}(z)$ satisfies the property

$$\boldsymbol{E}^t(z^{-1})\,\boldsymbol{E}(z) = \boldsymbol{I},$$

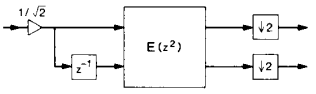

Fig. 7. The analysis bank.

which is called *paraunitariness* [16], [21] (if the factor β in Fig. 6 is dropped, then $\boldsymbol{E}(z)$ would satisfy $\boldsymbol{E}^t(z^{-1})\,\boldsymbol{E}(z) = c\boldsymbol{I}$ for a constant c).

In order to obtain perfect reconstruction, the synthesis filters should be taken as in (7) where $H_0(z)$ is $\hat{P}_{N-1}(z)$ and $H_1(z)$ is $\hat{Q}_{N-1}(z)$. From Fig. 1, we have

$$\begin{aligned} \hat{X}(z) &= \begin{pmatrix} F_0(z) & F_1(z) \end{pmatrix} \begin{pmatrix} Y_0(z) \\ Y_1(z) \end{pmatrix} \\ &= z^{-(N-1)} \begin{pmatrix} H_0(z^{-1}) & H_1(z^{-1}) \end{pmatrix} \begin{pmatrix} Y_0(z) \\ Y_1(z) \end{pmatrix}. \end{aligned}$$

But we know that

$$\begin{pmatrix} H_0(z) \\ H_1(z) \end{pmatrix} = \boldsymbol{E}(z^2) \begin{pmatrix} 1 \\ z^{-1} \end{pmatrix},$$

hence,

$$\begin{aligned} \hat{X}(z) &= z^{-(N-1)} \begin{pmatrix} 1 & z \end{pmatrix} \boldsymbol{E}^t(z^{-2}) \begin{pmatrix} Y_0(z) \\ Y_1(z) \end{pmatrix} \\ &= \begin{pmatrix} z^{-1} & 1 \end{pmatrix} z^{-2m_1} \boldsymbol{E}^t(z^{-2}) \begin{pmatrix} Y_0(z) \\ Y_1(z) \end{pmatrix} \end{aligned}$$

where $m_1 = (N-2)/2$. The complete analysis–synthesis system can therefore be drawn as in Fig. 8(a). The internal structure of $z^{-2m_1}\boldsymbol{E}^t(z^{-2})$, which we call the "transposed version" of the analysis lattice, is shown in Fig. 9.

The complete system in Fig. 8(a) is such that $\hat{x}(n) = c \cdot x(n-N+1)$ for all n, regardless of the values of α_m. Accordingly, if we optimize α_m so as to minimize the stopband energies of the analysis filters, then the optimization routine will automatically restrict its search to those transfer functions which satisfy the perfect-reconstruction property. This is the topic of the next section.

A second way to interpret the PCI property of Fig. 8(a) is this: based on standard identities [2], the structure can be redrawn as in Fig. 8(b). Since $\boldsymbol{E}(z)$ is paraunitary, the product $z^{-m_1}\boldsymbol{E}^t(z^{-1})\,\boldsymbol{E}(z)$ reduces to $cz^{-m_1}\boldsymbol{I}$ for some constant c, and hence, by inspection of Fig. 8(b), we get $\hat{x}(n) = \frac{1}{2}cx(n-2m_1-1)$.

IV. Determination of the Lattice Coefficients Using Optimization Techniques

The "desired frequency responses" of the transfer functions $\hat{P}_{N-1}(z)$ and $\hat{Q}_{N-1}(z)$ are of the form in Fig.

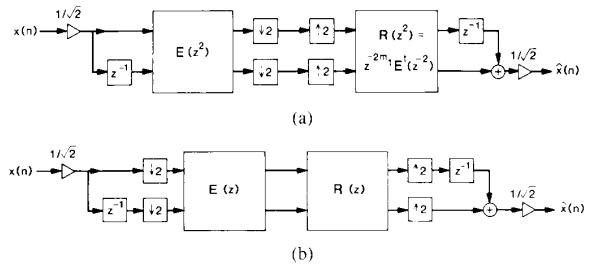

Fig. 8. (a) The complete QMF structure. (b) A redrawing of (a).

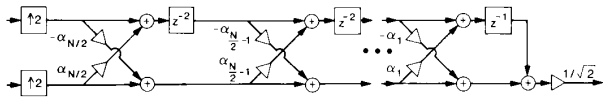

Fig. 9. Internal details of the synthesis bank.

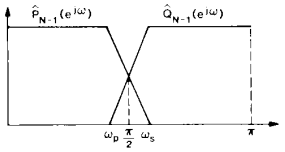

Fig. 10. Desired frequency responses of the lattice transfer functions.

10. Accordingly, we formulate an objective function

$$\Phi = \int_{\omega_s}^{\pi} \left| \hat{P}_{N-1}(e^{j\omega}) \right|^2 d\omega.$$

The parameter ω_s depends on the desired stopband edge of $\hat{P}_{N-1}(e^{j\omega})$. The objective function involves only the stopband energy of $\hat{P}_{N-1}(z)$. Since the lattice automatically ensures the relation (26), the stopband energy of $\hat{Q}_{N-1}(z)$ is equal to that of $\hat{P}_{N-1}(z)$ and is automatically minimized. Moreover, in view of the relation (25), a good stopband of $\hat{P}_{N-1}(z)$ ensures a "good passband" of $\hat{Q}_{N-1}(z)$, and vice versa. In summary, minimization of the above simple objective function ensures that $\hat{P}_{N-1}(z)$ and $\hat{Q}_{N-1}(z)$ are good low-pass and high-pass filters, respectively.

The "denormalized" lattice configuration is more suited for the nonlinear minimization problem than the normalized one, for two main reasons. First, if the normalized implementation is used, then additional constraints must be included so as to ensure that the coefficients k_m and $\hat{k}_m$ are bounded above by unity in magnitude, whereas the denormalized coefficients α_m have no constraint on their range of values. Second, computation of the objective function and its gradient based on α_m is less time consuming, because it involves a smaller number of square-roots[1] and simpler gradient expression. Note that even if k_m, $\hat{k}_m$ are expressed as $\cos\theta_m$, $\sin\theta_m$ to reduce the number of square roots and simplify the gradient expression, their computation is time consuming because, on most general-purpose computers, the sine and cosine are computationally as costly as the square root.

To solve the minimization problem, we invoked a subroutine called FMFP [18] which is based on the quasi-Newton method with Davidon–Fletcher–Powell update of the approximate Hessian matrix. As with most nonlinear optimization problems, the solution at convergence depends heavily on the initial parameter estimates.

The design results, presented in Tables I–VII, are obtained after solving the nonlinear minimization problem for various values of ω_s and $N - 1$. These tables have all the information required for most design applications. The method underlying these results is described in the rest of this section.

Hierarchical or Nesting Property of the Lattice: Any pair $\{P_m(z), Q_m(z)\}$ in Fig. 6 is a PCI pair. In the optimized QMF lattice, the purpose of each lattice section is to generate a better PCI pair $\{P_{m+2}(z), Q_{m+2}(z)\}$ (better in the sense of smaller stopband energy) from a given PCI pair $\{P_m(z), Q_m(z)\}$. As we progress toward the right in Fig. 6, we get better and better PCI pairs (and α_m gets smaller and smaller in magnitude for large m). This is an important *hierarchical* or *nesting* property of the lattice: if we delete the rightmost lattice section, we do not destroy the perfect-reconstruction property, but only decrease the available stopband attenuation of the analysis filters. Such a nesting property is of course not displayed by the direct-form implementation of a PCI pair.

Initial Estimates Using Method of Direct Differentiation: Since the number of coefficients α_m is large for high-order filters $P_{N-1}(z)$, it is difficult to obtain an optimal solution in a reasonable amount of time, starting from a random guess of their values. By "optimal solution" we mean a filter which is close to the one obtained from the Smith–Barnwell procedure [4], and which possesses the maximum possible number of zeros on the unit circle (see Appendix A). We found that, with a systematic way of computing the initial estimates, an optimal solution could always be obtained.

In view of the hierarchical property of the QMF lattice, we obtain an initial estimate of the coefficients α_m one at a time starting from the left of the lattice in Fig. 6. Since one variable is optimized at a time, each step can be done by direct differentiation. With each pair of "unscaled" transfer functions $\{P_{2m-1}(z), Q_{2m-1}(z)\}$, $m = 1, 2, \cdots, N/2$, in Fig. 6, let us associate a pair of "scaled" transfer functions $\{\hat{P}_{2m-1}(z), \hat{Q}_{2m-1}(z)\}$ defined as $\{\hat{P}_{2m-1}(z) = (\beta_m/\sqrt{2})\, P_{2m-1}(z)$ where $\beta_m^2 = \Pi_{i=1}^{m} (1 + \alpha_i^2)^{-1}$. Suppose that the first $m - 1$ coefficients $\{\alpha_1, \cdots, \alpha_{m-1}\}$ are known ($m > 1$), hence, the unscaled transfer functions $P_{2m-3}(z)$ and $Q_{2m-3}(z)$ are known. We want to determine α_m such that

$$\Phi_m = \int_{\omega_s}^{\pi} \left| \hat{P}_{2m-1}(e^{j\omega}) \right|^2 d\omega$$

$$= \frac{\beta_m^2}{2} \int_{\omega_s}^{\pi} \left| P_{2m-1}(e^{j\omega}) \right|^2 d\omega \qquad (27)$$

[1]On most general-purpose computers, computation of square roots and transcendental functions takes much longer time than add/multiply operations.

is minimized. The lattice upward recursion gives

$$P_{2m-1}(z) = P_{2m-3}(z) - \alpha_m z^{-2} Q_{2m-3}(z) \quad (28a)$$

$$Q_{2m-1}(z) = \alpha_m P_{2m-3}(z) + z^{-2} Q_{2m-3}(z). \quad (28b)$$

From (27) and (28), $\Phi_m = (\mathcal{A} + \alpha_m^2 \mathcal{B} - 2\alpha_m \mathcal{C})\, \beta_m^2/2$, where

$$\mathcal{A} = \int_{\omega_s}^{\pi} \left| P_{2m-3}(e^{j\omega}) \right|^2 d\omega,$$

$$\mathcal{B} = \int_{\omega_s}^{\pi} \left| Q_{2m-3}(e^{j\omega}) \right|^2 d\omega,$$

$$\mathcal{C} = \tfrac{1}{2} \int_{\omega_s}^{\pi} \left\{ e^{j2\omega} P_{2m-3}(e^{j\omega})\, Q_{2m-3}(e^{-j\omega}) + e^{-j2\omega} P_{2m-3}(e^{-j\omega})\, Q_{2m-3}(e^{j\omega}) \right\} d\omega.$$

If $\mathcal{C}$ is equal to zero, then $\alpha_m = 0$ would minimize Φ_m. Otherwise, we set

$$\frac{\partial \Phi_m}{\partial \alpha_m} = \frac{\beta_m^2}{1 + \alpha_m^2} \left\{ \mathcal{C}\alpha_m^2 - (\mathcal{A} - \mathcal{B})\alpha_m - \mathcal{C} \right\}$$

to zero, and obtain two roots

$$\text{root}_1 = \frac{\mathcal{A} - \mathcal{B}}{2\mathcal{C}} + \sqrt{\left(\frac{\mathcal{A} - \mathcal{B}}{2\mathcal{C}}\right)^2 + 1} > 0$$

$$\text{root}_2 = \frac{\mathcal{A} - \mathcal{B}}{2\mathcal{C}} - \sqrt{\left(\frac{\mathcal{A} - \mathcal{B}}{2\mathcal{C}}\right)^2 + 1} < 0.$$

Since $\partial \Phi_m / \partial \alpha_m$ is of the same sign as $\mathcal{C}$ for $\alpha_m \le \text{root}_2$ or $\alpha_m \ge \text{root}_1$ and of the opposite sign of $\mathcal{C}$ for $\text{root}_2 < \alpha_m < \text{root}_1$, the objective function Φ_m is minimal at $\alpha_m = \text{root}_1$ if $\mathcal{C}$ is strictly positive, and at $\alpha_m = \text{root}_2$ if $\mathcal{C}$ is strictly negative.

To start the above recursive procedure from no known coefficients, α_1 is set to be -1, since a quick calculation would show that

$$\Phi_1 = \int_{\omega_s}^{\pi} \left| \hat{P}_1(e^{j\omega}) \right|^2 d\omega = \int_{\omega_s}^{\pi} \frac{1}{\alpha_1^2 + 1} (\alpha_1^2 - 2\alpha_1 \cos\omega + 1)\, d\omega$$

is minimal at this value of α_1.

Using the described method, we were able to find up to 21 initial estimates of α_m, which were then taken as inputs to the quasi-Newton routine and subsequently led to an optimal solution. The resulting analysis filters are then of order $2(21) - 1 = 41$. A larger number of initial estimates obtained from the above method, e.g., 33, does not lead to an optimal solution. Therefore, in order to design filters of order higher than 41, we used the optimal set of α_m corresponding to a filter of lower order, e.g., 41, having the same ω_s, as the first part of an ordered set of initial estimates, then augmented it by a few more coefficients α_m (about 3 or 4) using the method described previously, then used this new set of α_m as input to the quasi-Newton routine to obtain a new optimal solution of higher order; the process was then repeated if the desired order had not been reached. We augmented a known set of α_m by only a few more at a time because a large number of added α_m might lead to a suboptimal solution.

We also have tried to adjust the set of initial estimates of α_m before invoking the quasi-Newton routine, by optimizing one α_m at a time, from the leftmost end of Fig. 6, keeping other coefficients fixed. This procedure is slightly more complicated. The improvement on the final objective function is not substantial.

Nonlinear Optimization Techniques: There is a wide variety of nonlinear optimization techniques to choose from. We selected the quasi-Newton method because, for this method, the number of iterations needed for convergence was relatively small (although each iteration might be more time consuming than that of other methods such as the conjugate-gradient technique). We also have tried the conjugate-gradient method by invoking the routine ZXCGR of the IMSL software package [19], and it resulted in an optimal solution similar to the one obtained with the quasi-Newton method. Both methods require the information on the gradient of Φ. This can be computed without invoking approximate first-difference techniques, by directly differentiating with respect to the lattice parameters, as follows. From the lattice structure, we get

$$\begin{pmatrix} P_{N-1}(z) \\ Q_{N-1}(z) \end{pmatrix} = \frac{1}{\sqrt{2}} \boldsymbol{V}(z^2) \cdot \begin{pmatrix} 1 & -\alpha_m z^{-2} \\ \alpha_m & z^{-2} \end{pmatrix} \boldsymbol{S}(z^2) \begin{pmatrix} 1 \\ z \end{pmatrix}$$

where $\boldsymbol{V}(z^2)$ and $\boldsymbol{S}(z^2)$ are 2×2 matrices of polynomials whose coefficients are functions of $\{\alpha_{N/2}, \alpha_{(N/2)-1}, \cdots, \alpha_{m+1}\}$, and $\{\alpha_{m-1}, \alpha_{m-2}, \cdots, \alpha_1\}$, respectively, and can be computed using the lattice upward recursion (28). This implies

$$\begin{pmatrix} \partial P_{N-1}(z)/\partial \alpha_m \\ \partial Q_{N-1}(z)/\partial \alpha_m \end{pmatrix} = \frac{1}{\sqrt{2}} \boldsymbol{V}(z^2) \begin{pmatrix} 0 & -z^{-2} \\ 1 & 0 \end{pmatrix} \boldsymbol{S}(z^2) \begin{pmatrix} 1 \\ z \end{pmatrix}.$$

From (27), we have

$$\frac{\partial \Phi}{\partial \alpha_m} = \int_{\omega_s}^{\pi} \left[\frac{\partial P_{N-1}(e^{-j\omega})}{\partial \alpha_m} P_{N-1}(e^{j\omega}) + P_{N-1}(e^{j\omega}) \frac{\partial P_{N-1}(e^{-j\omega})}{\partial \alpha_m} \right] d\omega.$$

The above integrand can be easily computed as the cross correlation of $P_{N-1}(e^{j\omega})$ and $\partial P_{N-1}(e^{j\omega})/\partial \alpha_m$. Thus, the gradient of Φ can be directly computed.

Design Example: The specifications for the filter $\hat{P}_{N-1}(z)$ are: order $= N - 1 = 47$ (i.e., there are $N/2 = 24$ coefficients α_m), $\omega_s = 0.6\pi$. First, we solved an auxiliary lower order filter problem with the same ω_s: 21 initial estimates of α_m were computed using the method

of direct differentiation described earlier, and were used as inputs to the quasi-Newton routine to subsequently produce the coefficients of the optimal filter of order $2(21) - 1 = 41$. Then, adding to this list of resulting coefficients three more coefficients α_m using the method of direct differentiation, we obtain 24 initial estimates of α_m for the original design problem. Again, the quasi-Newton routine was invoked, which finally returned the lattice coefficients for the optimal filter $\hat{P}_{47}(z)$.

Fig. 11 shows the magnitude response of $\hat{P}_{47}(e^{j\omega})$ and $\hat{Q}_{47}(e^{j\omega})$ in decibels. As expected, the passbands of the filters are extremely good (even though this is not the primary concern in QMF applications). The minimum attenuation in the stopband is 70 dB. The filter, with the same order and ω_s, as returned by the Smith–Barnwell scheme based on spectral factorization of an equiripple half-band filter, would theoretically have an attenuation of 72 dB in its equiripple stopband.

Figs. 12 and 13 depict the magnitude responses of $\hat{P}_{47}(e^{j\omega})$ after a 5-bit quantization, using signed-digit code, of the lattice coefficients α_m and of the impulse response coefficients, respectively. From these plots, the effect of quantization seems to be the same for both cases in the stopband region. But a magnification of the plot of $|\hat{P}_{47}(e^{j\omega})|^2 + |\hat{Q}_{47}(e^{j\omega})|^2$ (see Fig. 14) clearly shows the superior performance of the lattice: it retains the power-complementary property after quantization while the direct-form implementation does not. Hence, the PCI condition is satisfied by the QMF lattice even after quantization. This suggests that, for a prespecified quantization level, it might be possible to obtain a better QMF lattice by solving the nonlinear optimization problem with the variables α_m constrained to be powers-of-two or sums of powers-of-two. This aspect is currently under investigation.

Fig. 15 shows the magnitude response of the filter having the same order as the previous example, i.e., 47, but with ω_s equal to 0.62π. Notice that, in this case, the minimum stopband attenuation is 85 dB. The filter with the same order and ω_s, as returned by the Smith–Barnwell scheme, would have a theoretical stopband attenuation of 86 dB.

From Fig. 12, we observe that the passband sensitivity is extremely good. But it should be noticed that, for QMF applications, the stopband sensitivity is more important than the passband sensitivity. In Appendix B, we show that the lattice has approximately the same relative error in the stopband as in the passband; however, this fact does not imply that it has good stopband sensitivity.

Other design examples are summarized in the form of convenient design tables in Tables I–VII, a subset of which has essentially the same specifications, i.e., filter length and transition bandwidth, as the ones given by Johnston [13]. For ease of comparison, the filters in this subset are also denoted by the same filter numbers as the ones in [13]. Although the lattice filters outperformed the filters in [13] in regard to stopband attenuation, the reader should keep in mind that, for a filter length of N, the filters

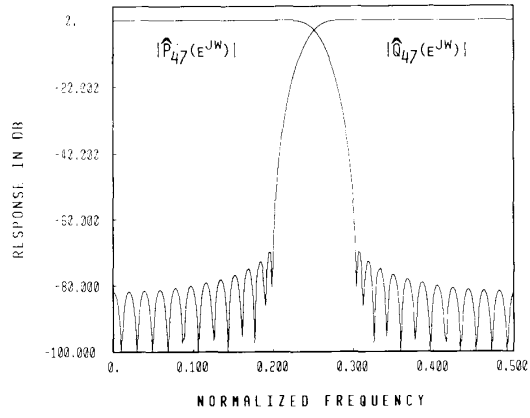

Fig. 11. Plot of $|\hat{P}_{47}(e^{j\omega})|$ and $|\hat{Q}_{47}(e^{j\omega})|$, with $\omega_s = 0.6\pi$.

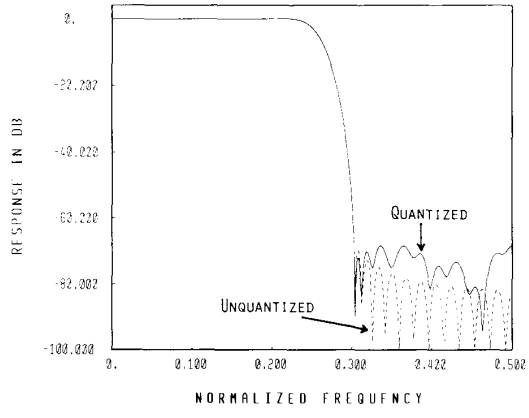

Fig. 12. Plot of $|\hat{P}_{47}(e^{j\omega})|$ after 5-bit quantization of the lattice coefficients.

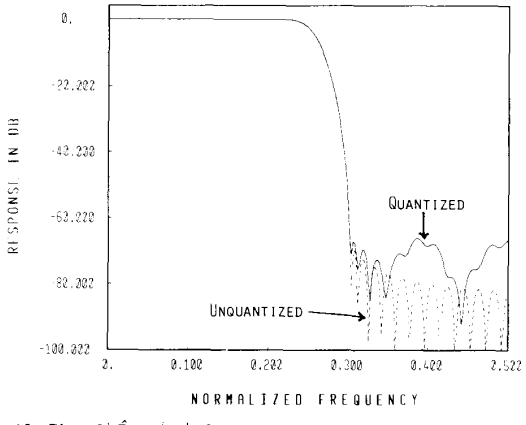

Fig. 13. Plot of $|\hat{P}_{47}(e^{j\omega})|$ after 5-bit quantization of the impulse response coefficients.

in [13] require only $N/2$ multipliers for implementing both $H_0(z)$ and $H_1(z)$, while the lattice filters require N multipliers. This, of course, is the price paid for the PCI property.

The reason we tabulate the lattice coefficients α_m, and

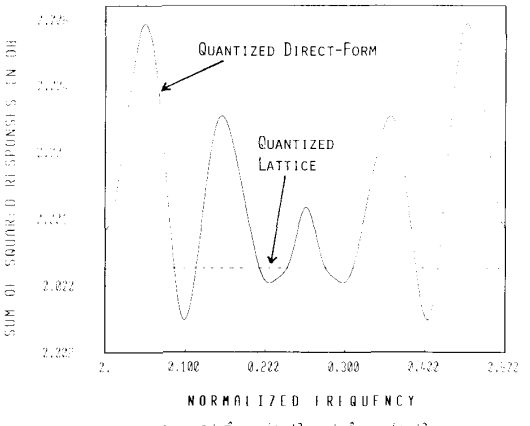

Fig. 14. Plot of $|\hat{P}_{47}(e^{j\omega})|^2 + |\hat{Q}_{47}(e^{j\omega})|^2$.

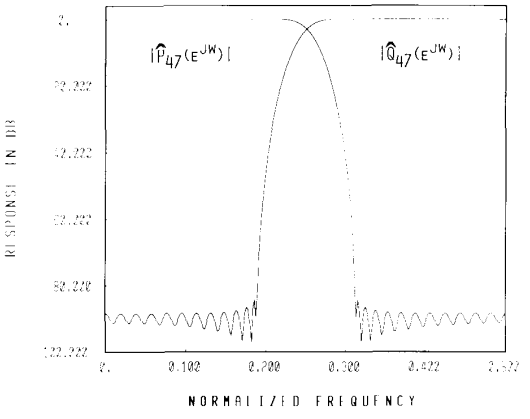

Fig. 15. Plot of $|\hat{P}_{47}(e^{j\omega})|$ and $|\hat{Q}_{47}(e^{j\omega})|$, with $\omega_s = 0.62\pi$.

not the impulse response coefficients, is because the α_m specify the lattice more concisely and, with the same number of precision bits, allow a more accurate computation of the impulse response coefficients (by way of a simple software program which is provided in Appendix C). Moreover, roundoff errors in α_m do not affect the PCI property.

V. Noise Analysis

We are interested in determining the noise variance at the output of the two-channel QMF structure of Fig. 8, where the analysis and synthesis banks are as in Figs. 6 and 9, respectively. In order to reduce the probability of internal signal overflow, the scaled version of the lattice should be used. In this configuration, β is decomposed into $N/2$ factors of the form $1/\sqrt{\alpha_i^2 + 1}$, where each factor is associated with the appropriate lattice section, as shown in Fig. 16. The transfer matrix of this section is

$$\boldsymbol{T}_i(z) = \frac{1}{\sqrt{1 + \alpha_i^2}} \begin{pmatrix} 1 & -\alpha_i z^{-2} \\ \alpha_i & z^{-2} \end{pmatrix} = \begin{pmatrix} k_{2i-1} & -\hat{k}_{2i-1} z^{-2} \\ \hat{k}_{2i-1} & k_{2i-1} z^{-2} \end{pmatrix},$$

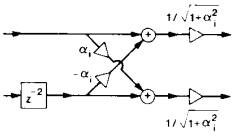

Fig. 16. A scaled lattice section of the analysis bank.

which can be verified to be paraunitary (i.e., $\boldsymbol{T}_i^t(z^{-1})\,\boldsymbol{T}_i(z) = \boldsymbol{I}$). In practice, the scale factors $1/\sqrt{1 + \alpha_i^2}$ are replaced with simple sums of powers-of-two to reduce the multiplier count, but we shall assume, for simplicity of analysis, that $\boldsymbol{T}_i(z)$ is indeed of the above form.

Assuming fixed-point arithmetic and that quantizers are inserted prior to each lattice section in the analysis bank and after each lattice section in the synthesis bank, we have the noise model of Fig. 17. As per usual assumptions [20], we assume the noise sources to be uncorrelated, zero-mean, and white, with variance σ^2 each. These assumptions continue to be true as long as the signal variance is considerably larger than the noise variance [25] (this, in turn, is true provided the wordlengths used for filtering operations are not excessively small).

The effect of the first noise source $e_1(n)$ can be determined separately as follows. Since the complete QMF structure inherently has the perfect-reconstruction property, the contribution of $e_1(n)$ to the total output noise is clearly equal to $\sqrt{2}e_1(n - N + 1)$. Referring to Fig. 17, the effect of each pair of noise sources $\{e_i(n), b_i(n)\}$, $i = 2, \cdots, N$, on the total output noise signal can be considered independently for each i. For the moment, let us ignore the presence of the decimators and interpolators. Consider the noise sources $\{e_i(n), b_i(n)\}$ located at the inputs of lattice section i (or at its outputs if it is a section in the synthesis bank, i.e., if $i > N/2$). Let $\{e_{i,\text{out}}(n), b_{i,\text{out}}(n)\}$ be the noise signals that appear at the outputs of lattice section number N, as a result of $\{e_i(n), b_i(n)\}$. The transfer matrix of the cascade of lattice sections numbered i (or $i + 1$, if $i > N/2$) through N is paraunitary since it is a product of paraunitary matrices.[2] It can be verified that, because of this paraunitary property, the resulting noise signals $\{e_{i,\text{out}}(n), b_{i,\text{out}}(n)\}$ are uncorrelated, zero-mean, and white, with the same variance σ^2 (see Appendix D). Now, in the absence of the decimators and interpolators, the total noise signal at the output of the complete QMF structure is

$$e(n) = \sqrt{2}e_1(n - N + 1) + \frac{1}{\sqrt{2}} \cdot \sum_{i=2}^{N} \left(e_{i,\text{out}}(n) + b_{i,\text{out}}(n)\right) + e_{N+1}(n).$$

Since all the noise sources $e_i(n)$, $b_i(n)$, $2 \le i \le N$, are pairwise uncorrelated, the resulting noise signals $e_{i,\text{out}}(n)$

[2]Depending on the value of i, this cascade comprises either some sections of the analysis bank and the whole synthesis bank, or the whole synthesis bank, or just part of the synthesis bank. However, these details are irrelevant to our derivation.

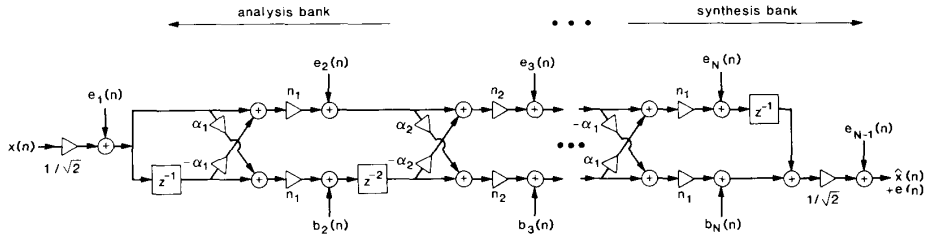

Fig. 17. The noise model for the complete QMF structure.

and $b_{i,\text{out}}(n)$, $2 \le i \le N$, are also pairwise uncorrelated. Therefore, it is clear that $E[e(n)] = 0$ and $\sigma_e^2 = (N + 2)\,\sigma^2$, where $E[\cdot]$ denotes the expected value, and σ_e^2 denotes the variance of $e(n)$.

Now, consider the decimators. Since they only compress the time axis, and since the noise signals entering them are assumed to be wide-sense stationary, the statistics of the noise signals are unaffected by them. Next, consider the interpolators at the inputs of the synthesis bank. Even if the input sequence to an interpolator is wide-sense stationary, the output is not wide-sense stationary since it contains a well-defined subsequence of zeros. To circumvent this problem in the noise analysis, we can redraw the complete QMF structure as in Fig. 18. Essentially, we replace the double delay of each internal lattice section of the block $\boldsymbol{R}(z^2) = z^{-(N-2)}\boldsymbol{E}^t(z^{-2})$ by a single delay. Let $e_{\text{out}}(n)$ and $b_{\text{out}}(n)$ be the noise signals that appear at the outputs of $\boldsymbol{R}(z)$ in Fig. 18, as a result of all internal noise sources [except $e_1(n)$]. Based on the above reasoning, we then have

$$E[e_{\text{out}}(n)] = E[b_{\text{out}}(n)] = 0,$$

$$R_{e_{\text{out}}e_{\text{out}}}(n_1, n_2) = R_{b_{\text{out}}b_{\text{out}}}(n_1, n_2) = (N - 1)\,\sigma^2\delta(n_1 - n_2)$$

where $R(\cdot, \cdot)$ is the autocorrelation. The contribution of this to that total output noise is

$$e'(n) = \begin{cases} \dfrac{1}{\sqrt{2}}\, e_{\text{out}}\left(\dfrac{n-1}{2}\right) & \text{if } n \text{ is odd;} \\ \dfrac{1}{\sqrt{2}}\, b_{\text{out}}\left(\dfrac{n}{2}\right) & \text{if } n \text{ is even.} \end{cases}$$

In general, $e'(n)$ is not wide-sense stationary since its autocorrelation depends on the parities of the sample numbers, but for this particular case where $e_{\text{out}}(n)$ and $b_{\text{out}}(n)$ are white, uncorrelated, have zero mean and the same variance, $e'(n)$ is also white, has zero mean and a variance equal to $\sigma^2(N - 1)/2$. Adding to this variance the ones contributed by e_{N+1} and the noise signal resulting from $e_1(n)$, which are σ^2 and $2\sigma^2$, respectively, we obtain the total output noise variance. In conclusion, the total roundoff noise variance at the location of the reconstructed signal $\hat{x}(n)$, due to all noise sources internal to the QMF bank, is $\sigma^2((N - 1)/2 + 3)$.

Coding Noise: In any practical application of the QMF bank, the decimated versions of the signals $x_0(n)$, $x_1(n)$ (Fig. 1) are encoded using one of many standard techniques [22]. The coding is usually done at a much coarser level than the quantization during filtering. Such coding noise sources cannot be modeled as additive uncorrelated white noise sources. Consequently, the above results do not apply in this case.

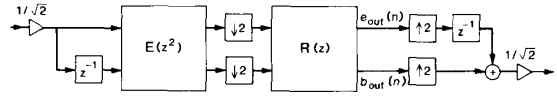

Fig. 18. An equivalent complete QMF structure.

VI. Concluding Remarks

In this paper, a structure and an algorithm have been presented for the design of two-channel QMF banks satisfying the sufficient conditions of perfect reconstruction introduced in [4]. The structure automatically satisfies these sufficient conditions, while the algorithm ensures a good stopband attenuation for each of the analysis filters $H_k(z)$. The results obtained by using the algorithm for various values of stopband frequency ω_s and filter order $N - 1$ are tabulated in Tables I–VII; these design tables are provided as a quick design aid, to save the designer from recomputing standard coefficients by complex optimization algorithms.

It will be of interest to restrict the lattice coefficients to be powers-of-two, and perform a "discrete space optimization," so as to obtain computationally efficient analysis bank structures. The basic nature of the lattice guarantees perfect reconstruction even with such powers-of-two coefficients.

It is easy to see that, with FIR analysis and synthesis filters, the PCI property [i.e., (7) and (8)] is not necessary for the perfect-reconstruction (PR) property. From Fig. 8(b), we see that a more general sufficient condition for perfect reconstruction is $\boldsymbol{R}(z)\,\boldsymbol{E}(z) = z^{-k}\boldsymbol{I}$. For example, if $\boldsymbol{E}(z)$ is FIR with $\det[\boldsymbol{E}(z)]$ equal to a delay, it is trivial to see that $\boldsymbol{R}(z) = z^{-k}\text{Adj}\,\boldsymbol{E}(z)$ will lead to the PR property (Adj denoting the adjugate or cofactor matrix).

Next, in all the schemes discussed here and in [4], it is true that $\boldsymbol{E}(z)$ is lossless. The losslessness condition on $\boldsymbol{E}(z)$ means that $H_0(z)$ and $H_1(z)$ are power complementary, and so cannot *both* have linear phase [24]. As indicated above, losslessness of $\boldsymbol{E}(z)$ and the relations in (7) are not necessary conditions for PR property. In fact, with

det $[E(z)]$ equal to a delay but $E(z)$ not lossless, one can obtain linear-phase analysis filters, and design examples can be found in [23]. However, the attenuation characteristics of these design examples are poorer than those of the class of filters without linear-phase constraint, first introduced in [4].

For the linear-phase case, perhaps the most judicious and practical scheme would be to use any of the techniques proposed over the last decade [1]–[3], [13]–[15], which do not insist on theoretical perfect reconstruction. These techniques are such that aliasing and phase distortion are completely eliminated (in spite of multiplier quantization) and amplitude distortion is minimized in a systematic fashion [13], [14]. In applications where linearity of phase of the analysis filters is important, these earlier techniques seem to be most promising.

Appendix A

Let N_{zeros} be the maximum number of zeros that $\hat{P}_{N-1}(z)$ can have on the unit circle. Recall that $N-1$ is odd. It can be shown that if $N/2$ is even, then $N_{\text{zeros}} = N/4$, and if $N/2$ is odd, then there are two cases:

a) $N_{\text{zeros}} = (N+2)/4$ if $\hat{P}_{N-1}(e^{j\omega})$ has a zero at $\omega = \pi$, and

b) $N_{\text{zeros}} = (N-2)/4$ if $\hat{P}_{N-1}(e^{j\omega})$ does not have a zero at $\omega = \pi$.

The proof is as follows. Let $\hat{P}_{N-1}(z)$ be a spectral factor of $G_+(z)$ (25). $G_+(z)$ and $G(z)$ are shown in Fig. 2. Figuratively speaking, $G_+(e^{j\omega})$ is obtained from $G(e^{j\omega})$ by "pushing" the curve upward by an amount of δ. It is clear from Fig. 2 that $G_+(e^{j\omega})$ has only double zeros, and the number of the double zeros, N_{dz}, which is equal to the number of zeros of $\hat{P}_{N-1}(e^{j\omega})$, is related to the number of zeros of the derivative of $G(e^{j\omega})$. Since $G(z)$ is a linear phase FIR filter, we have $G(e^{j\omega}) = \sum_{n=0}^{N-1} c_n(\cos\omega)^n$. This implies

$$G'(e^{j\omega}) = \frac{dG(e^{j\omega})}{d\omega} = -\sin\omega \sum_{n=1}^{N-1} nc_n(\cos\omega)^{n-1}. \quad \text{(A.1)}$$

Let $N_{G'}$ be the number of zeros of $G'(e^{j\omega})$ in the interval $[0, \pi]$, and N_s denote the number of zeros of $G'(e^{j\omega})$ in the interval $[\omega_s, \pi]$. Since $G(e^{j\omega})$ is a half-band filter, we have $N_{G'} = 2N_s$. In (A.1), the term $\sin\omega$ contributes two zeros, while the sum term contributes a maximum of $N-2$ zeros. Thus, N_s can be at most $(2 + (N-2))/2 = N/2$.

Suppose that $G(e^{j\omega})$ has no zero at $\omega = \pi$. If N_s is even, this means that $G(e^{j\omega})$ is positive at $\omega = \pi$ and has $N_s/2$ extrema of value $-\delta$. Thus, after "pushing" the curve up by δ, there is no zero at $\omega = \pi$, and $N_{dz} = N_s/2$ which is at most equal to $N/4$. If N_s is odd, then $G(e^{j\omega})$ is negative at $\omega = \pi$ and has $(N_s+1)/2$ extrema of value $-\delta$. Thus, after "pushing" it up by δ, there is a double zero at $\omega = \pi$, and $N_{dz} = (N_s+1)/2$ which has a maximum value of $(N+2)/4$.

Suppose that $G(e^{j\omega})$ has a zero at $\omega = \pi$ (necessarily a double zero since $G(z)$ is linear phase and has even order). After "pushing" it up by δ, there is no zero at $\omega = \pi$. If N_s is even, then $G(e^{j\omega})$ is negative near $\omega = \pi$, and has $N_s/2$ extrema of value $-\delta$. Thus, $N_{dz} = N_s/2$. If N_s is odd, then $G(e^{j\omega})$ is positive near $\omega = \pi$, and has $(N_s-1)/2$ extrema of value $-\delta$. So, $N_{dz} = (N_s-1)/2$ which is at most equal to $(N-2)/4$. This concludes the proof.

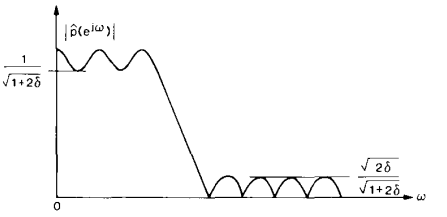

Fig. 19. Pertaining to Appendix B.

Appendix B

Consider the half-band filter $G_+(e^{j\omega})$ shown in Fig. 2. The filter $\hat{P}_{N-1}(e^{j\omega})$, obtained by spectral factorizing the normalized $G_+(e^{j\omega})$, is as shown in Fig. 19. Let $2\delta_1$ and $2\delta_2$ be the peak-to-peak ripples in the passband and stopband, respectively. From Fig. 19, we have $1 - 2\delta_1 = 1/\sqrt{1+2\delta}$, $\delta_2 = \sqrt{2\delta}/\sqrt{1+2\delta}$. Thus, $2\delta = 1/(1-2\delta_1)^2 - 1$. This implies $\delta_2 = 2\sqrt{\delta_1 - \delta_1^2} \approx 2\sqrt{\delta_1}$. Let $2\delta_1'$ and $2\delta_2'$ be the new peak-to-peak ripples, resulting from quantization of the lattice coefficients. Typically, we will have $\delta_1' \geq \delta_1$ and $\delta_2' \geq \delta_2$. Let $\epsilon_1 = \delta_1' - \delta_1$ and $\epsilon_2 = \delta_2' - \delta_2$. The relative errors in ripple sizes are $\epsilon_1/\delta_1 = (\delta_1' - \delta_1)/\delta_1 = \delta_1'/\delta_1 - 1$, $\epsilon_2/\delta_2 = (\delta_2' - \delta_2)/\delta_2 = \delta_2'/\delta_2 - 1 \approx \sqrt{\delta_1'/\delta_1} - 1$. Thus, $\epsilon_2/\delta_2 \approx \sqrt{\epsilon_1/\delta_1 + 1} - 1$. Since the lattice has low passband sensitivity [6], $\epsilon_1/\delta_1 \ll 1$, hence, $\sqrt{\epsilon_1/\delta_1 + 1} \approx 1 + \epsilon_1/2\delta_1$. In other words, $\epsilon_2/\delta_2 \approx \epsilon_1/2\delta_1$, which shows that the relative change in the stopband ripple size is only half as much as that in the passband. This, however, does not imply that ϵ_2 itself is "small;" although we cannot conclude that the stopband sensitivity is low, we do obtain an upper bound on the quantity ϵ_2.

Appendix C

```
c*************************************************************
c this subroutine computes the coefficients of P(z) and Q(z)
c from a set of alphas. Inputs and outputs are in single precision.
c inputs  : array alpha(n), n
c outputs: coefficients of P(z) and Q(z) in the arrays p(2n), q(2n)
c*************************************************************
```

```
      subroutine getpq(alpha, n, p, q)
      real*4 p(n + n),q(n + n),pold(100),qold(100)
      real*4 alpha(n)

      n2 = n + n
c compute scale factor
      prod = alpha(1)*alpha(1) + 1.
      do 10 i = 2, n
      prod = prod*(alpha(i)*alpha(i)+1.)
 10   continue
      beta = sqrt(0.5/prod)
      pold(1) = 1.
      pold(2) = -alpha(1)
      qold(1) = alpha(1)
      qold(2) = 1.
      m=2
      p(1) = pold(1)
      p(2) = pold(2)
      do 40 j=4, n2, 2
      q(1) = alpha(m)*pold(1)
      q(2) = alpha(m)*pold(2)
      if (j.eq.4) goto 22
      do 20 i=3, j-2
        p(i) = pold(i) - alpha(m)*qold(i-2)
        q(i) = alpha(m)*pold(i) + qold(i-2)
 20   continue
 22   do 25 i=j-1, j
        p(i) = -alpha(m)*qold(i-2)
        q(i) = qold(i-2)
 25   continue
      do 30 i=1, j
        pold(i) = p(i)
        qold(i) = q(i)
 30   continue
      m=m+1
 40   continue
      do 50 i=1, n2
        p(i) = beta*p(i)
        q(i) = beta*p(i)
 50   continue
      return
      end
```

Appendix D

Let $e_0(n)$ and $e_1(n)$ be two uncorrelated, zero-mean, white random processes [20]. Let $\sigma^2 = E[e_0^2(n)] = E[e_1^2(n)]$ be the common variance. Clearly, $e_0(n)$ and $e_1(n-2)$ are also uncorrelated. Defining $\boldsymbol{e}(n) = [e_0(n)\ e_1(n-2)]^t$ to be a vector-random process, its covariance matrix is

$$\boldsymbol{C}(n, n') = E[\boldsymbol{e}(n)\,\boldsymbol{e}^t(n')] = \sigma^2 \boldsymbol{I}\delta(n - n'). \quad \text{(A.2)}$$

If we now define $\boldsymbol{f}(n) = \boldsymbol{R}\boldsymbol{e}(n)$ to be a new vector-random process, then

$$E[\boldsymbol{f}(n)\boldsymbol{f}^t(n')] = \boldsymbol{R}E[\boldsymbol{e}(n)\,\boldsymbol{e}^t(n')]\boldsymbol{R}^t = \boldsymbol{R}\boldsymbol{C}(n, n')\boldsymbol{R}^t = \sigma^2\boldsymbol{R}\boldsymbol{R}^t. \quad \text{(A.3)}$$

If $\boldsymbol{R}$ is orthogonal, i.e., $\boldsymbol{R}\boldsymbol{R}^t = \boldsymbol{R}^t\boldsymbol{R} = \boldsymbol{I}$, then

$$E[\boldsymbol{f}(n)\boldsymbol{f}^t(n')] = \sigma^2\boldsymbol{I}\delta(n - n'), \quad \text{(A.4)}$$

that is, the components of $\boldsymbol{f}(n)$ are white and uncorrelated, and have equal variance σ^2.

By repeated application of these principles in Fig. 17, we can verify that every pair of noise sources $\{e_i(n), b_i(n)\}$ creates a pair of uncorrelated white noise signals $\{e_{i,\text{out}}(n), b_{i,\text{out}}(n)\}$ of equal variance σ^2 at the two output terminals of the Nth lattice section.

References

[1] D. Esteban and C. Galand, "Application of quadrature mirror filters to split-band voice coding schemes," in *Proc. IEEE Int. Conf. Acoust., Speech, Signal Processing*, Hartford, CT, May 1977, pp. 191-195.

[2] R. E. Crochiere and L. R. Rabiner, *Multirate Digital Signal Processing*. Englewood Cliffs, NJ: Prentice-Hall, 1983.

[3] C. R. Galand and H. J. Nussbaumer, "New quadrature mirror filter structures," *IEEE Trans. Acoust., Speech, Signal Processing*, vol. ASSP-32, pp. 522-531, June 1984.

[4] M. J. T. Smith and T. P. Barnwell, III, "Exact reconstruction techniques for tree-structured subband coders," *IEEE Trans. Acoust., Speech, Signal Processing*, vol. ASSP-34, pp. 434-441, June 1986. (Basic results presented at the IEEE Int. Conf. Acoust., Speech, Signal Processing, San Diego, CA, Mar. 1984.)

[5] K. Swaminathan and P. P. Vaidyanathan, "Theory and design of uniform DFT, parallel quadrature mirror filter banks," *IEEE Trans. Circuits Syst.*, vol. CAS-33, pp. 1170-1191, Dec. 1986.

[6] P. P. Vaidyanathan, "Passive cascaded lattice structures for low sensitivity FIR filter design, with applications to filter banks," *IEEE Trans. Circuits Syst.*, vol. CAS-33, pp. 1045-1064, Nov. 1986.

[7] J. H. Rothweiler, "Polyphase quadrature filters: A new subband coding technique," in *Proc. 1983 IEEE Int. Conf. Acoust., Speech, Signal Processing*, Boston, MA, Mar. 1983, pp. 1280-1283.

[8] P. L. Chu, "Quadrature mirror filter design for an arbitrary number of equal bandwidth channels," *IEEE Trans. Acoust., Speech, Signal Processing*, vol. ASSP-33, pp. 203-218, Feb. 1985.

[9] M. Vetterli, "Filter bank allowing perfect reconstruction," *Signal Processing*, vol. 10, no. 3, pp. 219-266, Apr. 1986.

[10] F. Mintzer, "Filters for distortion-free two-band multirate filter banks," *IEEE Trans. Acoust., Speech, Signal Processing*, vol. ASSP-33, pp. 626-630, June 1985.

[11] P. P. Vaidyanathan, "Theory and design of M-channel maximally decimated quadrature mirror filters with arbitrary M, having the perfect reconstruction property," *IEEE Trans. Acoust., Speech, Signal Processing*, vol. ASSP-35, pp. 476-492, Apr. 1987.

[12] M. J. T. Smith and T. B. Barnwell, III, "A unifying framework for analysis/synthesis systems based on maximally decimated filter banks," in *Proc. IEEE Int. Conf. Acoust., Speech, Signal Processing*, Tampa, FL, Mar. 1985, pp. 521-524.

[13] J. D. Johnston, "A filter family designed for use in quadrature mirror filter banks," in *Proc. IEEE Int. Conf. Acoust., Speech, Signal Processing*, Apr. 1980, pp. 291-294.

[14] V. K. Jain and R. E. Crochiere, "Quadrature mirror filter design in the time-domain," *IEEE Trans. Acoust., Speech, Signal Processing*, vol. ASSP-32, pp. 353-361, Apr. 1984.

[15] T. P. Barnwell, III, "Subband coder design incorporating recursive quadrature filters and optimum ADPCM vocoders," *IEEE Trans. Acoust., Speech, Signal Processing*, vol. ASSP-30, pp. 751-765, Oct. 1982.

[16] P. P. Vaidyanathan and S. K. Mitra, "Low passband sensitivity digital filters: A generalized viewpoint and synthesis procedures," *Proc. IEEE*, vol. 72, pp. 404-423, Apr. 1984.

[17] P. P. Vaidyanathan, S. K. Mitra, and Y. Neuvo, "A new approach to the realization of low-sensitivity IIR digital filters," *IEEE Trans. Acoust., Speech, Signal Processing*, vol. ASSP-34, pp. 350-361, Apr. 1986.

[18] J. L. Kuester, *Optimization Techniques with Fortran*. New York: McGraw-Hill, 1973.

[19] The IMSL Library: A set of Fortran subroutines for mathematics and statistics, IMSL Inc., Houston, TX.

[20] A. V. Oppenheim and R. W. Schafer, *Digital Signal Processing*. Englewood Cliffs, NJ: Prentice-Hall, 1975.
[21] V. Belevitch, *Classical Network Synthesis*. San Francisco, CA: Holden-Day, 1968.
[22] N. S. Jayant and P. Noll, *Digital Coding of Waveforms*. Englewood Cliffs, NJ: Prentice-Hall, 1984.
[23] M. Vetterli, "A theory of multirate filter banks," *IEEE Trans. Acoust., Speech, Signal Processing*, vol. ASSP-35, pp. 356–372, Mar. 1987.
[24] P. P. Vaidyanathan, "On power-complementary FIR filters," *IEEE Trans. Circuits Syst.*, vol. CAS-32, pp. 1308–1310, Dec. 1985.
[25] C. W. Barnes, B. N. Tran, and S. H. Leung, "On the statistics of fixed-point roundoff error," *IEEE Trans. Acoust., Speech, Signal Processing*, vol. ASSP-23, pp. 595–606, June 1985.

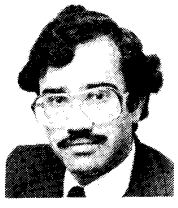

P. P. Vaidyanathan (S'80–M'83) was born in Calcutta, India, on October 16, 1954. He received the B.Sc. (Hons.) degree in physics and the B.Tech. and M.Tech. degrees in radiophysics and electronics from the University of Calcutta, India, in 1974, 1977, and 1979, respectively, and the Ph.D. degree in electrical and computer engineering from the University of California, Santa Barbara, in 1982.

He was a Postdoctoral Fellow at the University of California, Santa Barbara, from September 1982 to February 1983. Since March 1983 he has been with the California Institute of Technology, Pasadena, as an Assistant Professor of Electrical Engineering. His main research interests are digital signal processing, linear systems, and filter design.

Dr. Vaidyanathan served as the Vice Chairman of the Technical Program Committee for the 1983 IEEE International Symposium on Circuits and Systems. He currently serves as an Associate Editor for the IEEE TRANSACTIONS ON CIRCUITS AND SYSTEMS. He was the recipient of the Award for Excellence in Teaching at the California Institute of Technology for 1983/84. He was also a recipient of the National Science Foundation's Presidential Young Investigator Award, starting from the year 1986.

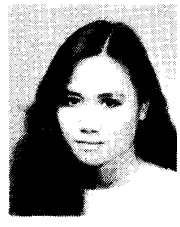

Phuong-Quan Hoang (S'84) was born in Danang, Vietnam, on January 1, 1955. She received the B.S.E.E. degree (summa cum laude) from the University of Lowell, Lowell, MA, in 1977, the M.S. and Engineer degrees in electrical engineering and computer science from the Massachusetts Institute of Technology, Cambridge, in 1981 and 1982, respectively.

She is currently working toward the Ph.D. degree in electrical engineering at the California Institute of Technology, Pasadena. From 1982 to 1986 she was a member of the Technical Staff at Hughes Aircraft Company, Fullerton, CA, initially full time, then part time. Her main research interests are in digital signal processing and filter designs.

Ms. Hoang was a recipient of the Hughes Doctoral Fellowship.